Polarimetric photoluminescence microscope for strain imaging on semiconductor devices

Emmanuel Schaub, Brahim Ahammou, Jean-Pierre Landesman

Polarimetric photoluminescence microscope for strain imaging on semiconductor devices

EMMANUEL SCHAUB,[1,*] BRAHIM AHAMMOU,[2,3] AND JEAN-PIERRE LANDESMAN[2]

[1]*Univ Rennes, CNRS, Intitut de Physique de Rennes – UMR 6251, F-35000 Rennes, France*
[2]*Univ Rennes, INSA Rennes, CNRS, Institut FOTON–UMR 6082, F-35000 Rennes, France*
[3]*Department of Engineering Physics and Centre for Emerging Device Technologies, McMaster University, Hamilton, ON, L8S 4L7, Canada*
**emmanuel.schaub@univ-rennes1.fr*

Abstract: Anisotropic strain induces a partial linear polarization of the photo-luminescence (PL) emitted by cubic semiconductor crystals such as GaAs or InP. We present here a polarimetric PL microscope dedicated to the characterization of semiconductor devices. The anisotropic strain is quantified through the determination of the degree of linear polarization (DOLP) of the PL and of the angle of this partial linear polarization. We illustrate the possibilities of this tool by mapping the anisotropic strain generated in GaAs by the presence of a stressor film at its surface, i.e. a microstructure defined in a dielectric thin film (SiNx) which has been deposited with a built-in stress and shaped into a narrow stripe by lithography and etching. Our setup shows a DOLP resolution as low as 4.5×10^{-4} on GaAs.

1. Introduction

Strain mapping and imaging in semiconductor devices has been an active field over the years mainly for two reasons. First, mechanical stress, which is associated to strain, is one of the major causes, generally speaking, for device degradation and the resulting limitation of devices reliability [1]. Second, strain engineering strategies are being used and developed in a number of semiconductor devices nowadays to improve their performance [2]. In this article, we focus on the question of mapping strain in the semiconductor material itself, whereas a given device or module usually includes a semiconductor chip, wires or other types of electrical connections, a package, all of which can be highly sensitive to mechanical stress.

To map strain in semiconductor materials or devices, one is looking for an experimental technique providing the best sensitivity, spatial resolution and, if possible, some flexibility for investigating various components of the strain tensor. This last point is very important in particular when considering the possible role of shear stresses in degradation mechanisms. Various experimental techniques are available for strain mapping in semiconductor materials with the request of high sensitivity to strains, high spatial resolution, and sometimes sensitivity to various elements of the strain tensor. Starting with what is probably the most powerful class of techniques in terms of the above requirements, we mention transmission electron microscopy which has been widely used to address the topic [3]. Different approaches for the processing of high resolution transmission electron microscopy have been developed to produce local strain maps with very high accuracy [4] such as dark field electron holography, high resolution imaging, nano-beam electron diffraction. The major limitation is the need to prepare a very thin slab (in the order of 100 nm in thickness) of the semiconductor material, with very high accuracy in the selection of the area within the device to be investigated, and of course the necessity to have access to high-end electron microscopes with

highly skilled people operating them. Also becoming part of the high performance techniques in this field of research are the X-ray nano-diffraction instruments [5] but these instruments make use of synchrotron radiation centers which somewhat limits their accessibility. Then comes a class of optical spectroscopy techniques that have demonstrated their efficiency to solve a number of stress / strain related problems in semiconductor device technology. Micro-Raman spectroscopy [6] has allowed understanding the role of shear stresses induced in the silicon material for example by local oxidation techniques (used to provide electrical isolation between metal-oxide semiconductor field effect transistors at the surface of an integrated circuit). The spatial resolution for this kind of technique is not as good as what is reached with electron microscopy, but the instruments are much easier to operate, and the implementation does not require any specific fancy sample preparation process. The experimental approach is based on the measurement of the spectral shift of the Raman lines, which is mainly determined by the hydrostatic part of the crystal deformation (local volume change) but was also shown to be sensitive to other elements of the strain tensor such as shear strain. Polarization-dependent optical second-harmonic generation (SHG) [7], and third harmonic generation (THG) [8] can also be used to measure local strain properties in two-dimensional (2D) materials. While SHG is limited to non-centrosymmetric material, THG is in principle applicable to any 2D crystalline materials. However, these techniques require femtosecond laser sources. When possible, optical transmission through the semiconductor material can be used, and this signal will be sensitive only to the anisotropic part of the strain tensor which induces birefringence through the photo-elastic effect [9] . Micro-photoluminescence (µPL) can also be used as demonstrated by [10,11]. Similar to micro-Raman, the information on strain is deduced from the spectral shift of the PL signal, which makes this technique essentially sensitive to the hydrostatic part. It should be noticed, however, that micro-Raman as well as µPL can only be applied to specific semiconductor materials, having non-zero Raman efficiency or direct band-gap (for the case of µPL). Cassidy and co-workers [15] have developed a variant approach of µPL where, instead of analyzing spectra, the spectrally integrated signal is analyzed for its degree of polarization (DOP). DOP is sensitive to the anisotropic part of the strain tensor, while insensitive to the isotropic (or hydrostatic) part. This approach has proven particularly efficient for the analysis of situations where the semiconductor crystal deformation is dominated by this anisotropic part [12–15]. DOP has a very good sensitivity to small anisotropic deformations, as is the case for semiconductors such as GaAs, InP and the associated ternary and quaternary compounds, which have small yield stresses.

In this work, we developed a new acquisition setup, the straightforward signal analysis of which highlights the local strain tensor in terms of anisotropic strain and principal axes orientation. Thus, for the first time, we show maps of the degree of linear polarization (DOLP) of the PL, which is proportional to the anisotropic strain as well as orientation maps of the linear component of the PL polarization state, which is a principal axis of the strain. We reached a DOLP resolution of 4.5×10^{-4}.

2. Theory

Let us consider the configuration where the sample surface is defined as the xz plane and the direction perpendicular to this surface as the y direction (fig.**1**). We assume in the following that the strain information is mapped in the xz plane, by scanning of the sample along the two directions in this plane, thanks to focalization of a laser beam propagating in the y direction.

The PL signal is collected in the backscattering geometry, i.e. in the (-y) direction . We will call xyz the “laboratory” coordinate system in the following.

At a given point M, we choose a local coordinate system $x'yz'$, which is such that $x'$and z' are aligned with the principal strain directions. There is necessarily one of these two principal directions for which the strain is greater than the other. We name x' the principal axis for which the strain is the greatest. In this coordinate system, the in-plane strain matrix writes [16]:

$$\begin{bmatrix} \epsilon_{x'x'} & 0 \\ 0 & \epsilon_{z'z'} \end{bmatrix}, \text{ with } \epsilon_{x'x'} > \epsilon_{z'z'} \quad (1)$$

Let $\beta_{x'} = \widehat{xx'}$.

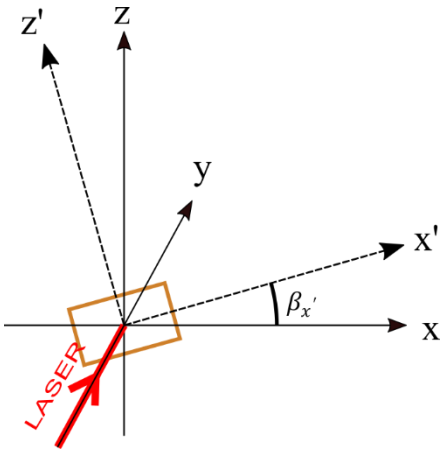

Fig.1. xyz laboratory axes coordinates, $\mathbf{x'z'}$ principal strain axes ($\boldsymbol{\epsilon_{x'x'} > \epsilon_{z'z'}}$).

2.1 Photoluminescence polarization state

In this part, we will first establish that, in the case of isotropic materials, the polarized component of the PL is necessarily linearly polarized along a principal axis of the strain tensor. By isotropic material in terms of strain induced PL polarization, we mean material for which the strain induced PL polarization state remains unchanged, when rotating by any angle the material orientation (the crystal axes for instance) about the y axis, all other things being equal (the strain being maintained unchanged). Then we discuss the case cubic crystal systems such as InP and GaAs. For this last material, polarization resolved PL maps will be presented in the experimental results part.

In any case, a partially polarized beam can be described as the superimposition of a fully depolarized beam and of a fully polarized beam [17]. The fully depolarized contribution is invariant by symmetry with respect to the strain principal axes x' and z'. A material which is isotropic in the absence of strain becomes anisotropic in the presence of anisotropic strain. In this case, x' and z' are symmetry axes of the system. As a consequence, the polarized component of the beam, which is induced by the anisotropic strain, must also remain unchanged by these symmetries. In the most general case, the polarization of the polarized component is elliptical. Only ellipses with axes aligned with respect to x' and z' are invariant by symmetries with respect to x' and z'. However, the rotation direction of the ellipse is reversed. As a consequence, the polarized beam has no choice but to be linearly polarized

either along x' or along z'. As shown later, the indeterminacy between these two cases can be removed experimentally.

GaAs is not an isotropic material, it is a cubic crystal. As was experimentally established by Cassidy and co-workers on GaAs [15,18], due to the presence of anisotropic strain, the PL beam which was non-polarized in the initial cubic crystal becomes partially linearly polarized. In the case of cubic crystals, the number of plane symmetry operations is 9. If, on the probed surface of the sample, a strain principal axis coincides with one of the symmetry plane, the system remains invariant by symmetry with respect to x' and z'. For the same reasons as in the case of an isotropic material, in this specific case, the linearly polarized component must be along x' or along z'. For other principal axis strain directions, this last statement is a simplifying assumption, which has to be verified experimentally. As shown in the result part, in the case of GaAs, the PL is aligned along z', the axis of lowest strain.

2.2 Principle of the experimental measurement

In this part, we will show how the analysis of the PL polarization allows us to characterize the strain in the material.

For that purpose, we use a linear polarizer (analyzer), rotating at a constant speed. The rotation frequency is f_M. We detect the intensity of the beam transmitted by the analyzer: I(t). Experimentally, at each point of our region of interest (ROI), we record I(t) for a given acquisition time. The mapping procedure consists in keeping the optical path fixed while scanning the sample using two high accuracy mechanical steppers along the x and z directions. The full I(t) signal, acquired over a time interval of typically 100 ms, is thus recorded at each location of the ROI. The step size is chosen according to the scale of the details to be analyzed. The minimal step size is 0.25 µm, which is determined taking into account the laser beam diameter (in the order of 1 µm). With this step size, ROIs of 200x200 μm^2 can be recorded.

2.3 Determination of the PL polarization angle θ

Let I_{np} (resp. I_p) be the intensity of the fully depolarized (resp. polarized) beam. We measure the PL polarization angle with respect to the vertical direction z. Let α be the polarizer angle with respect to the vertical direction z (fig. 2).

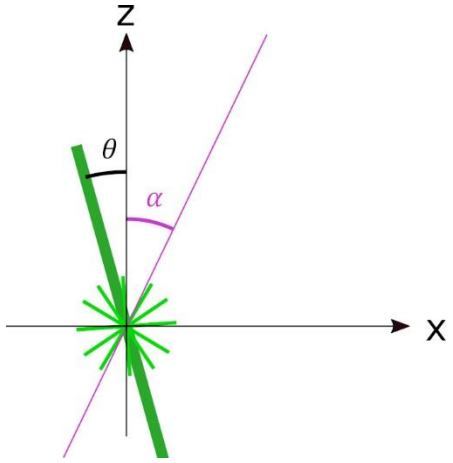

Fig.2. Angle θ: polarisation direction of the PL with respect to z, α angle of the analyzer with respect to z. The green star represents the fully depolarized component of the PL. The green stroke represents the polarized component of the PL.

On fig. 2, α is the angle of the analyzer with respect to the z axis, and θ is the polarization angle of the linear component of the PL with respect to the z axis. By projection of the fully depolarized component of the PL and of the linear component of the PL on the analyzer axis, we deduce the intensity transmitted by the analyzer:

$$I = \frac{1}{2}I_{np} + I_p \cos^2(\alpha - \theta) = \frac{1}{2}\left(I_{np} + I_p\right) + \frac{1}{2}I_p\cos\left(2(\alpha - \theta)\right) \quad (2)$$

The polarizer is rotating at a constant frequency f_M: $\alpha(t) = 2\pi f_M t + \alpha_0$,
where α_0 is the angle position for $t = 0$.

$$I(t) = DC + A\cos(4\pi f_M t + \phi), \quad (3)$$

with $DC = \frac{1}{2}\left(I_{np} + I_p\right)$, $A = \frac{1}{2}I_p$, and $\phi = 2\alpha_0 - 2\theta$

The frequency of $I(t)$ is twice that of the motor.

From the measurement of ϕ we can determine directly θ, the angle of the PL:

$$\theta = \alpha_0 - \frac{1}{2}\phi \quad (4)$$

Knowing DC and A we will show in the next subsection how to determine the DOLP.

2.4 Determination of the DOLP

We express the Stokes parameters as a function of I_{np}, I_p, and θ [19]:

$$S_0 = I_{np} + I_p \quad (5)$$

$$S_1 = I\left(\alpha = \frac{\pi}{2}\right) - I(\alpha = 0) = \left(\frac{1}{2}I_{np} + I_p \sin^2\theta\right) - \left(\frac{1}{2}I_{np} + I_p \cos^2\theta\right)$$

$$S_1 = -I_p \cos 2\theta \quad (6)$$

$$S_2 = I\left(\alpha = -\frac{\pi}{4}\right) - I\left(\alpha = \frac{\pi}{4}\right) = \frac{1}{2}I_p\cos\left(2\left(-\frac{\pi}{4} - \theta\right)\right) - \frac{1}{2}I_p\cos\left(2\left(-\frac{\pi}{4} - \theta\right)\right)$$

$$S_2 = -I_p \sin 2\theta \quad (7)$$

$S_3 = 0$ in our case because we have shown that the polarized component of the beam is linearly polarized.

Thus our instrument is able to fully characterize the polarization state of the PL beam.

The degree of linear polarization is defined [20] as $DOLP = \frac{\sqrt{S_1^2 + S_2^2}}{S_0}$.

$$\mathrm{DOLP} = \frac{\mathrm{I_p}}{\mathrm{I_{np}+I_p}} = \frac{\mathrm{A}}{\mathrm{DC}} \tag{8}$$

2.5 Relations with strain tensor components

In this subsection we will express DOLP and θ as functions of the strain tensor components in the laboratory coordinate system xyz.

The rectilinear contribution of the PL is induced by anisotropic strain. In a first order approximation, the DOLP is proportional to $\epsilon_{x'x'} - \epsilon_{z'z'}$ [18], and the linear component of the PL is either in the x'direction or in the z' direction. This can be written:

$\mathrm{DOLP} = \mathrm{C_\epsilon}(\epsilon_{x'x'} - \epsilon_{z'z'})$, with $\mathrm{C_\epsilon}$ a positive constant.

We use the in-plane principal strains formulae [16]:

$$\epsilon_{x'x'} = \frac{1}{2}(\epsilon_{xx} + \epsilon_{zz}) + \sqrt{\frac{1}{4}(\epsilon_{xx} - \epsilon_{zz})^2 + \epsilon_{xz}^2} \tag{9}$$

$$\epsilon_{z'z'} = \frac{1}{2}(\epsilon_{xx} + \epsilon_{zz}) - \sqrt{\frac{1}{4}(\epsilon_{xx} - \epsilon_{zz})^2 + \epsilon_{xz}^2} \tag{10}$$

Thus, $\epsilon_{x'x'} - \epsilon_{z'z'} = \sqrt{(\epsilon_{xx} - \epsilon_{zz})^2 + 4\epsilon_{xz}^2}$

$$\mathrm{DOLP} = \mathrm{C_\epsilon}\sqrt{(\epsilon_{xx} - \epsilon_{zz})^2 + 4\epsilon_{xz}^2} \tag{11}$$

Using the in-plane principal directions formula:

$\tan 2\beta_{x'} = \frac{2\epsilon_{xz}}{\epsilon_{xx}-\epsilon_{zz}}$, with the constraint $\epsilon_{x'x'} \geq \epsilon_{z'z'}$. (12)

Let's find an expression of $\beta_{x'}$:

$$\text{Let } \beta_1 = \frac{1}{2}\arctan\frac{2\epsilon_{xz}}{\epsilon_{xx}-\epsilon_{zz}} \tag{13}$$

From the strain transformation formulae, we calculate ϵ'_{xx1} and ϵ'_{zz1} using β_1:

$\epsilon'_{xx1} = \epsilon_{xx}\cos^2\beta_1 + \epsilon_{zz}\sin^2\beta_1 + \epsilon_{xz}\sin 2\beta_1$

$\epsilon'_{zz1} = \epsilon_{xx}\sin^2\beta_1 + \epsilon_{zz}\cos^2\beta_1 - \epsilon_{xz}\sin 2\beta_1$

$$\text{If } (\epsilon'_{xx1} \geq \epsilon'_{zz1}) \text{ then } \beta_{x'} = \beta_1, \text{ else } \beta_{x'} = \beta_1 + \frac{\pi}{2} \tag{14}$$

As said before, depending on the material, the luminescence must be partially polarized either along the x' direction, or along z'. The choice between these two possibilities is determined experimentally. If the polarization is along the direction x', for which the strain is the greatest, $\theta = \beta_{x'} - \frac{\pi}{2}$. If the polarization is along the direction z', for which the strain is the least, $\theta = \beta_{x'}$.

In the case of GaAs, the luminescence gets partially polarized along z', the direction for which the strain is the least, as will be shown in the result part.

3. Experimental setup

3.1 Description of the setup

The experimental setup is represented fig. 3:

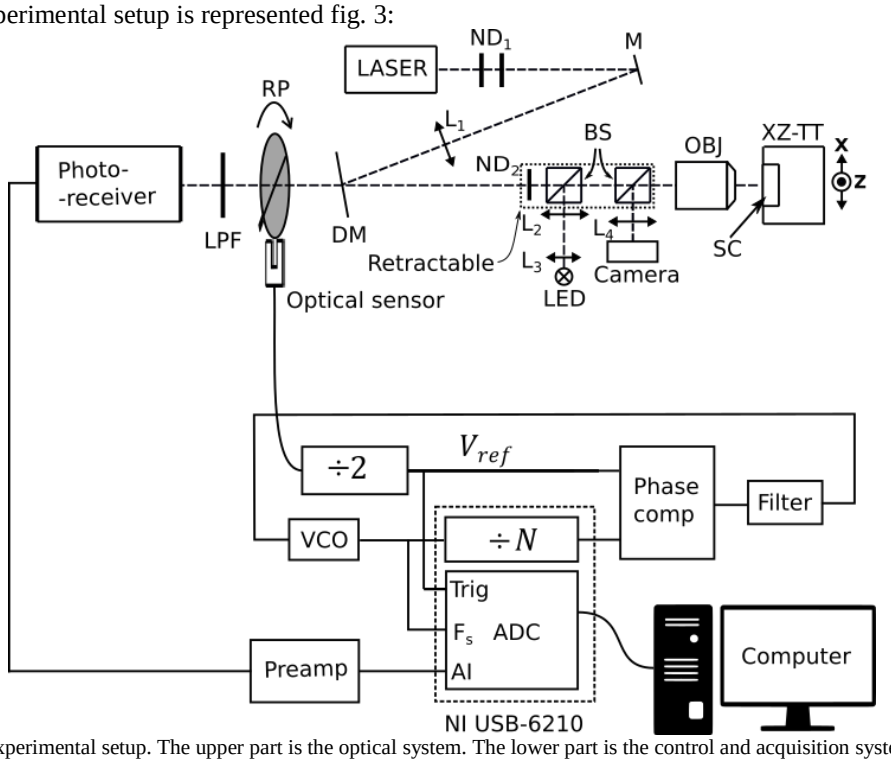

Fig.3. Experimental setup. The upper part is the optical system. The lower part is the control and acquisition system. **M**: mirror; **L_1, L_2, L_3, L_4**: lenses; **OBJ**: Objective lens; **SC**: semiconductor device;**XZ-TT**: motorized XZ translation table; **BS**: 50/50 beamsplitter cube; **ND_1**, **ND_2**: neutral density filters; **DM**: dichroic mirror; **RP**: rotating polarizer; **LPF**: long pass filter

The power of the 635nm, 5mW laser source (LabLaser CW, Coherent) is attenuated by a dual neutral density (ND) filter wheel (5215, New Focus). Typically, we use an optical density of 1.4. The 100mm focal length planconvex lens L focalizes the laser beam on the optical axis. The dichroic (cold) mirror (03MCS005, Melles Griot) reflects the laser beam which is directed toward the 0.4 NA microscope objective lens (M-20X, Newport). The beam is focalized onto the sample by the objective. The spot size is approximately 1µm. The focus of the laser beam can be adjusted by moving the objective lens along the optical axis. The sample is moved in the x and z direction by two high resolution translation stages. In order to check the focus and select the ROI, a visualization set consisting of an illumination white LED (MNWHL4, Thorlabs), two retractable 50/50 beam-splitters (BS), an optical density 3 ND filter and a color camera (DFK 42BUC03, Imagingsource) is used. During the PL measurement, the BSs are removed from the beam path. The induced PL is collected by the same objective lens. It is transmitted by the cold mirror. Then it travels through the linear polarizer. The linear polarizer is mounted on a brushless hollow shaft motor. The motor speed is constant and controlled by an electronic driver. Typically, the rotation frequency of the polarizer is $f_M = 112$ Hz. An optical sensor detects the passage of the polarizer at each turn

and provides pulses at frequency f_M. The PL beam passes through a long pass filter, whose purpose is to cut off the excitation laser. The PL is focused onto the photodiode active area of a home-made transimpedance photoreceiver. The signal at the output of the photoreceiver is amplified by a preamplifier (SR560, Stanford Reasearch Systems), the bandwidth of which is adjusted to 10kHz, 12dB/oct. The signal at the output of the preamplifier is sampled by an ADC (NI USB-6210, National Instruments).

We implemented a phase locked loop (PLL) control, for the sampling frequency to be an exact multiple of f_M, the rotation frequency of the analyzer. This way we can set the acquisition time for each pixel to be an integer number of motor rotations, and during a rotation we acquire an integer number of samples. The electronic chip we used to implement our PLL is a CD4046. It contains in particular a voltage controlled oscillator (VCO) and a phase comparator. In order to get a 50% duty cycle signal, we divide the frequency of the optical sensor by a factor of two. The resulting signal V_{ref} is used as the reference frequency for the PLL: $\nu_{ref} = \frac{f_M}{2} = 56$ Hz. A VCO is used as a clock source for the sampling of the PL signal. We denote ν_{VCO} the frequency of the VCO output signal. The center frequency of our VCO is approximately 220 kHz. Our DAQ (NI-USB 6210) is a multifunction DAQ. It is used as an analog to digital converter. It is also able to work as a frequency divider (DAQdiv). These two functions can be used simultaneously and are independent of each other. The VCO output frequency is divided by DAQdiv by a factor of $2P = 4000$. The frequency of the output signal of DAQdiv is ν_{comp}. An XOR gate based phase comparator compares the phase of the PLL reference signal with that of the output signal of DAQdiv. The phase comparator output is connected to the corrector filter, which controls the VCO. This way, the PLL controls the VCO frequency so that when it is locked, $\nu_{comp} = \nu_{ref}$. Moreover, the start of the acquisition is triggered by V_{ref}. At each pixel, we sample the PL signal during $n = 11$ motor revolutions. Thus the acquisition time is $t_{acq} = n / f_M = 98.2$ ms. $P = 2000$ is the number of points per motor revolution. Therefore the number of samples acquired at each pixel is: $N = nP = 11 \times 2000 = 22000$. For a motor speed of $f_M = 112$ Hz, the sampling frequency is $\nu_{VCO} = P\nu_P = 112 \times 2000 = 224$ kHz.

3.2 Signal analysis

Given that at each point the acquired signal consists of an integer number of motor periods n, each period consisting of P samples, the signal is first averaged over one period of time. Let $\{y_n\}$, with $0 \leq n < P$, be this averaged period.

The discrete Fourier transform of $\{y_n\}$ is processed by FFT:

$$Y_k = \sum_{n=0}^{P-1} y_n \exp\left(-i2\pi k \frac{n}{P}\right) \quad (15)$$

The inverse Fourier transform is $y_n = \frac{1}{P}\sum_{k=0}^{P-1} Y_k \exp\left(i2\pi n \frac{k}{P}\right)$ (16)

Referring to Eq. (3), we find:

$$DC = \frac{Y_0}{P} \quad (17)$$

$$A = \frac{2}{P}|Y_2| \tag{18}$$

$$\phi = \arg(Y_2) \tag{19}$$

As will be illustrated in the results section, from these three parameters we are able to plot three images of our ROI.

3.3 Offset and pick-up correction

To correct for the offset and the pick-up, a measurement $\{y_{Dark,n}\}$ is performed while blocking the laser. This background signal is first subtracted from the measurement at each pixel:

$$y_n = y_{Raw,n} - y_{Dark,n} \tag{20}$$

3.4 Bias correction

Even on a bare isotropic wafer, on which the PL is fully depolarized, we experimentally observe that $I_{exp}(t)$ undergoes a small periodical modulation at frequency f_M. We believe that this is due to a transmission of the polarizer not being uniform on its surface, so that the transmission depends on its orientation.

In this subsection, we will show that of the two parameters Y_0 and Y_2, required for the calculation of the DOLP and the angle θ, only Y_2 needs to be corrected, and we derive a simple formula for this correction.

The experimental signal we measure can be written as:

$I_{exp}(t) = I(t)(1 + \epsilon_T(t))$, where $I(t)$ is the unbiased signal. (21)

A measurement $\{y_{W,n}\}$ is performed on a uniform reference sample free of residual stresses (we used a GaAs bare wafer) and its FFT $\{Y_{W,n}\}$ is processed.

$$y_{W,n} = \langle y_{W,n} \rangle \left[1 + \epsilon_T \left(\frac{1}{f_M}\frac{n}{P}\right)\right] \tag{22}$$

$$\langle y_{W,n} \rangle = Y_{W,0} / P \tag{23}$$

On the device under test, $y_n = y_{C,n}\left[1 + \epsilon_T \left(\frac{1}{f_M}\frac{n}{P}\right)\right]$, with $y_{C,n}$ the unbiased signal. As $\epsilon_T \ll 1$, we have:

$$y_{C,n} \cong y_n \left[1 - \left(\frac{y_{W,n}}{\langle y_{W,n} \rangle} - 1\right)\right] \tag{24}$$

$$y_{C,n} \cong \left[\frac{Y_0}{P} + \frac{1}{P}\sum_{k=1}^{P-1} Y_k \exp\left(i2\pi n \frac{k}{P}\right)\right]\left[1 - \left(\sum_{k=1}^{P-1} \frac{Y_{W,k}}{Y_{W,0}} \exp\left(i2\pi n \frac{k}{P}\right)\right)\right] \tag{25}$$

For small values of $\frac{Y_{W,k}}{Y_{W,0}}$, $y_{C,n} \cong \frac{Y_0}{P} + \frac{1}{P}\sum_{k=1}^{P-1}\left(Y_k - \frac{Y_0 Y_{W,k}}{Y_{W,0}}\right)\exp\left(i2\pi n \frac{k}{P}\right)$ (26)

Finally:

$$Y_{C,0} = Y_0 \quad (27)$$

$$Y_{C,2} = Y_2 - Y_0 \frac{Y_{W,2}}{Y_{W,0}} \quad (28)$$

4. Samples preparation

In order to demonstrate the potential of our experimental set-up we designed samples based on GaAs substrates with a crystal deformation field induced by stressor dielectric films at their surface. In our case, the stressor is a SiN_x thin film deposited at the GaAs surface with a built-in stress resulting from the deposition process. We have already performed and published a detailed study of this kind of sample [13]. The SiN_x thin film is deposited using plasma enhanced chemical vapor deposition (PECVD) at 280 °C. The built-in stress in these thin films is adjusted by controlling the parameters of the PECVD process, such as the RF power fed into the reactor, and determined from measurements of the curvature of the GaAs wafer induced by the thin film deposition. The Stoney model [21] correlates the substrate curvature to the built-in stress within the thin film. We prepared SiN_x thin film with different built-in stresses: –293 MPa compressive films and 164 MPa tensile films.

After deposition, the SiN_x thin films (thickness: 500 nm) were structured into different geometrical shapes in order to produce various kinds of deformation fields within the underlying GaAs substrate, which were measured and mapped using our polarimetric PL microscope set-up. The mapped surface corresponds to the (001) crystal plane of the GaAs substrate. Elongated stripes with a width of 30 µm and a length of several mm, the direction of which corresponds to the [110] crystal direction of the GaAs substrate, as well as circles with a diameter of 30 µm were fabricated by optical lithography of a polymer resist deposited on top of the SiN_x thin film, opening of this polymer resist, and subsequent etching of the SiN_x thin film by plasma etching using SF_6. This procedure is described in details in [13].

5. Results

Figure 4 shows the maps obtained on a sample with a stripe made from a tensile SiN_x film deposited on a GaAs substrate. Figure 4(a) shows the average PL intensity. It is higher below the stripe. Several reasons might explain this higher intensity (optical anti-reflection effect of the SiN_x film or improvement of the GaAs surface quality below the SiN_x film). Figure 4(b) shows the DOLP in logarithmic scale. Its value is maximum at the edges of the stripe, both inside and outside. Far from the stripe remains only residual noise. Figure 4(c) shows the PL polarization angle θ. Below the stripe far from its end, the polarization is horizontal. Just outside the stripe, the polarization direction switches to vertical. The opposite occurs close to the stripe edge: vertical polarization below the stripe, becoming horizontal outside. In all cases near an edge, the polarization outside the stripe is perpendicular to that inside the stripe. Far from the stripe, the polarization tends to become random. Below the stripe, the tensile deformation within SiN_x induces a compressive deformation within the substrate material. On the other hand, because of the stripe form factor, the strain along the stripe should be negligible [14]. Thus we know that in this area (i.e. below the SiN_x stripe far from it's edge) the maximum principal strain is along z. Below the stripe, far from its end, the anisotropic strain of greatest extension x' is thus vertical. As the orientation of the linear polarization component of the PL is horizontal, we deduce that, in the case of GaAs, the polarization is along the principal axis of least strain. On the substrate, outside the stripe, far from its end, the stripe exerts a tension on the substrate, so that the anisotropic strain is here horizontal. The

linear polarization component of the PL is here vertical, which confirm that the polarization is along z', the least strain principal axis. At the horizontal edge of the stripe end, the compression induced by the stripe makes the anisotropic strain under the stripe horizontal, and thus the PL polarization is here vertical. On the other side of this border, outside the ribbon, it is the opposite, the tension induced by the stripe makes the anisotropic strain vertical, and thus the orientation of the linear polarization component of the photoluminescence is horizontal. In the upper part of the image, far from the structure, the DOLP is very weak and the PL angle becomes random. In figure 4(b), below the stripe, at a distance of about 15µm from the horizontal edge, the dark area shows a very weak DOLP. At this point the strain anisotropy is zero, which obviously does not mean that the strain is zero, since at this point the substrate is compressed. It simply means that at this point the strain is isotropic. In Fig. 4(b), in the region surrounded by a dashed rectangle (ROI), far from the structure, the signal arises from the noise. In this ROI, the mean DOLP is 4.5×10^{-4}, which is the resolution of our instrument on GaAs. Actually the DOLP and the angle θ result from a single complex value $Z = \mathrm{DOLP} \times \exp(2i\theta)$. The module of the mean complex value is 4.9×10^{-6}, which is much lower than the mean DOLP. Since in fig. 4(c) the angle is random in this ROI , this result is expected. It confirms that the effect of the strain on the PL signal is negligible with respect to the noise in this region.

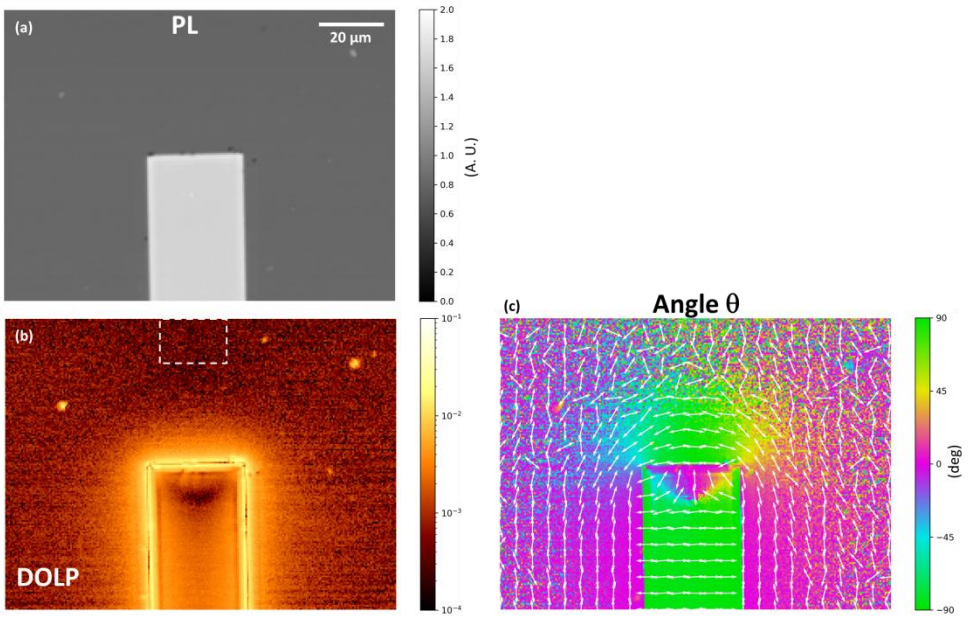

Fig.4. Mapping of a 30 µm tensely stressed SiNx stripe on a GaAs substrate. (a) Average PL intensity. (b) Degree Of Linear Polarization (DOLP). (c) Polarization angle of the linearly polarized component of the PL

Figure 5 shows the maps obtained on a sample with a disk made from a compressive SiN_x deposited on a GaAs substrate. Figure 5(a) shows the average PL intensity. It is higher at the disk and especially at its edge. Figure 5(b) shows the DOLP in logarithmic scale. Its value is maximum at the edge of the disk, both inside and outside. Far from the disk remains only residual noise. Figure 5(c) shows the PL polarization angle θ. Inside the disk, the polarization is azimuthal, while outside the disk the polarization is radial. As in the stripe case, near the edge, the polarization outside and inside the stripe is perpendicular to each other. Far from the

disk, the polarization tends to become random. At the center of the disk, the polarization tends to be random too. All maps, namely intensity map, DOLP and angle θ, seams to be circularly symmetrical. Inside the disk, we also see a small point, which is a defect, both on the DOLP image as well as on the θ image, which is not visible on the PL image.
Unlike the stripe of fig 4, which is a tensile film, the disk of figure 5 is a compressive film. As a consequence, below the disk, the compressive disk applies a tensile stress on the substrate. As a consequence, below the disk, the axis of greatest extension x' is radial. As in this region the polarization is azimuthal, we confirm that, on GaAs, the polarization is along the direction of least extension. The same is true outside the disk: in this region, the compressive disk applies a compressive stress on the substrate. The axis of greatest strain is azimuthal. As expected, the PL polarization is radial in this region. At the center of the disk the DOLP is zero and the phase random, which is expected for symmetry reasons. Again it does not mean that at this point the strain is zero, but that it is isotropic. In the theoretical part, we treated the case of an isotropic material in terms of strain-induced PL polarization state, and we pointed out that GaAs is a cubic crystal the strain-induced PL polarization property of which is not necessarily isotropic. The circular symmetry of our maps seems to indicate that the isotropy of GaAs in terms of strain induced polarization is valid.

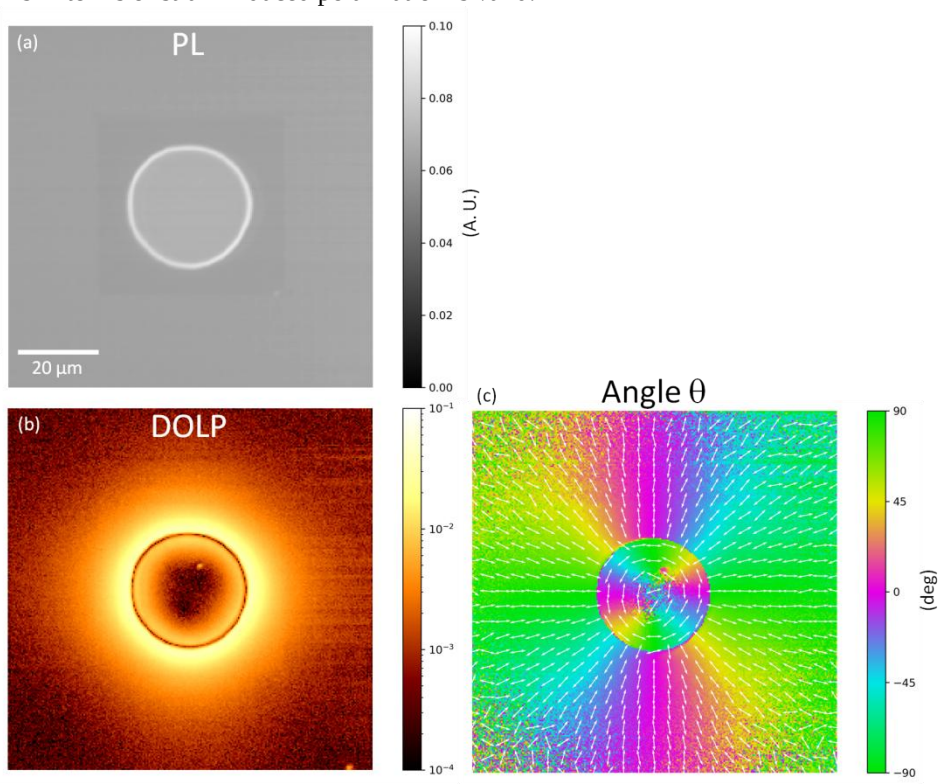

Fig.5. Mapping of a compressively stressed SiN_x disk on a GaAs substrate. (a) Average PL signal. (b) Degree Of Linear Polarization (DOLP). (c) Polarization angle of the linearly polarized component of the PL

6. Discussion and prospects

We compare here our approach with that introduced by Cassidy and co-workers0 [15]. In their work, the linear polarization of the PL is characterized by a "Degree Of Polarization"

(DOP) and a "Rotated degree Of Polarization" (ROP). One can show that these quantities are related to the Stokes parameters through the formulae:

$$\mathrm{DOP} = \mathrm{S}_1/\mathrm{S}_0 \quad (29)$$

$$\mathrm{ROP} = -\mathrm{S}_2/\mathrm{S}_0 \quad (30)$$

From Eq. (5-8), it can be shown that:

$$DOP = C_\epsilon \cos 2\theta \sqrt{(\epsilon_{xx} - \epsilon_{zz})^2 + 4\epsilon_{xz}^2} = DOLP \cos 2\theta \quad (31)$$

$$ROP = -C_\epsilon \sin 2\theta \sqrt{(\epsilon_{xx} - \epsilon_{zz})^2 + 4\epsilon_{xz}^2} = -DOLP \sin 2\theta \quad (32)$$

The fact to describe the polarization state in terms of DOLP and angle θ highlights the anisotropic strain as well as its principal axis, which is more meaningful for understanding the strain effect in the semiconductor notably for structures which are not either vertical or horizontal with respect to the laboratory axis.

From an experimental point of view, Cassidy and co-workers [15] use both a rotating analyzer as well as a mechanical chopper, while in our case we don't use a mechanical chopper. The purpose of the mechanical chopper is to reduce the noise induced by the ambient light. The rotation frequency of the analyzer and that of the chopper frequency are asynchronous. As a consequence, the signal is not periodical, which results in perturbations in the detected signal due to beating effects [22]. While these fluctuations can be minimized by adjusting empirically the rotation frequency of the analyzer, the procedure is tricky, and not stable in time. On the other hand information concerning the luminescence signal is distributed over a complicated signal spectrum, while the signal analysis procedure only extract the complex amplitude at the chopper frequency and that at twice the analyzer rotation frequency. In our case all the information is contained in the DC component and in the second harmonic of the spectrum. In addition, our measurements are also perfectly reproducible. However, it requires that the signal be measured in dark, and the photo-receiver as well as the preamplifier must allow the DC component. As explained before, in our case, the DC offset also needs to be compensated.

In addition, in this work we established a method for compensating for systematic errors which are characterized by the fact that even on an isotropic sample, the PL signal is modulated. In the previous method, this signal modulation could be partially reduced by adjusting the position of the analyzer. But the procedure was tricky, and it was not possible to fully cancel the residual modulation.

In the present work, the master clock is the rotation frequency of the motor, and the sampling frequency has been set to a multiple of the motor rotation frequency. A more elegant alternative could be to use the sampling frequency as the master clock (synchronized with respect to the quartz clock), in which case the motor speed would be controlled to a sub-multiple of the sampling frequency. In this case, a specific motor controller should be designed. The advantage would be that the sampling frequency be perfectly stable. However, we don't think that at the end, we would see any difference in the images.

With our current setup, the measurement time is limited both by the signal acquisition time and the motor displacement time. More precisely, the acquisition time is approximately

100ms/point. The measurement time for a cartography of 241x241 points is 13600s (approx. 3h 47mn), which gives a ratio between the cartography measurement time and it number of points of approximately 230ms/point, which means that the time required for the sample motion is comparable to that of the acquisition time. We are working on reducing this measurement time. Several solution have been identified.

7. Conclusion

We developed a polarimetric PL microscope, dedicated to the characterization of anisotropic strain on semiconductor devices. It provides mapping of the DOLP, which is proportional to the anisotropic strain, as well as the orientation of the linear component of the luminescence, which is a principal axis of the strain. We believe that this instrument will be very useful in optimizing the fabrication processes of direct band-gap semiconductor device, both to improve their reliability as well as their specifications.

8. Disclosures

The authors declare no conflicts of interest.

9. Data availability

Data underlying the results presented in this paper are not publicly available at this time but may be obtained from the authors upon reasonable request.

References

1. S. Yang, D. Xiang, A. Bryant, P. Mawby, L. Ran, and P. Tavner, "Condition Monitoring for Device Reliability in Power Electronic Converters: A Review," IEEE Trans. Power Electron. **25**, 2734–2752 (2010).
2. D. J. Paul, "Si/SiGe heterostructures: from material and physics to devices and circuits," Semicond. Sci. Technol. **19**, R75–R108 (2004).
3. M. Hÿtch, F. Houdellier, F. Hüe, and E. Snoeck, "Nanoscale holographic interferometry for strain measurements in electronic devices," Nature **453**, 1086–1089 (2008).
4. A. Béché, J. L. Rouvière, J. P. Barnes, and D. Cooper, "Strain measurement at the nanoscale: Comparison between convergent beam electron diffraction, nano-beam electron diffraction, high resolution imaging and dark field electron holography," Ultramicroscopy **131**, 10–23 (2013).
5. T. Stankevič, E. Hilner, F. Seiboth, R. Ciechonski, G. Vescovi, O. Kryliouk, U. Johansson, L. Samuelson, G. Wellenreuther, G. Falkenberg, R. Feidenhans'l, and A. Mikkelsen, "Fast Strain Mapping of Nanowire Light-Emitting Diodes Using Nanofocused X-ray Beams," ACS Nano **9**, 6978–6984 (2015).
6. I. De Wolf, H. E. Maes, and S. K. Jones, "Stress measurements in silicon devices through Raman spectroscopy: Bridging the gap between theory and experiment," Journal of Applied Physics **79**, 7148–7156 (1996).
7. J. Liang, J. Zhang, Z. Li, H. Hong, J. Wang, Z. Zhang, X. Zhou, R. Qiao, J. Xu, P. Gao, Z. Liu, Z. Liu, Z. Sun, S. Meng, K. Liu, and D. Yu, "Monitoring Local Strain Vector in Atomic-Layered MoSe2 by Second-Harmonic Generation," Nano Lett. **17**, 7539–7543 (2017).

8. J. Liang, J. Wang, Z. Zhang, Y. Su, Y. Guo, R. Qiao, P. Song, P. Gao, Y. Zhao, Q. Jiao, S. Wu, Z. Sun, D. Yu, and K. Liu, "Universal Imaging of Full Strain Tensor in 2D Crystals with Third-Harmonic Generation," Adv. Mater. **31**, 1808160 (2019).
9. E. Hecht, "Chap 8.11.1: Photoelasticity," in *Optics* (Pearson Education Limited, 2017).
10. J.-P. Landesman, "Micro-photoluminescence for the visualisation of defects, stress and temperature profiles in high-power III–V's devices," Materials Science and Engineering: B **91–92**, 55–61 (2002).
11. J. Jimenez and J. W. Tomm, *Spectroscopic Analysis of Optoelectronic Semiconductors*, Springer Series in Optical Sciences (Springer International Publishing, 2016), Vol. 202.
12. S. Gerard, M. Mokhtari, J.-P. Landesman, C. Levallois, M. Fouchier, E. Pargon, P. Pagnod-Rossiaux, F. Laruelle, A. Moreac, B. Ahammou, and D. T. Cassidy, "Photoluminescence mapping of the strain induced in InP and GaAs substrates by SiNx stripes etched from thin films grown under controlled mechanical stress," Thin Solid Films **706**, 138079 (2020).
13. M. Mokhtari, P. Pagnod-Rossiaux, F. Laruelle, J.-P. Landesman, A. Moreac, C. Levallois, and D. T. Cassidy, "Optical Characterizations of VCSEL for Emission at 850 nm with Al Oxide Confinement Layers," J. Electron. Mater. **47**, 4987–4992 (2018).
14. M. Mokhtari, P. Pagnod-Rossiaux, C. Levallois, F. Laruelle, D. T. Cassidy, M. Bettiati, and J.-P. Landesman, "Mechanical strain mapping of GaAs based VCSELs," Applied Physics Letters **118**, 091102 (2021).
15. D. T. Cassidy, S. K. K. Lam, B. Lakshmi, and D. M. Bruce, "Strain mapping by measurement of the degree of polarization of photoluminescence," Appl. Optics **43**, 1811–1818 (2004).
16. P. Kelly, "4.2 Plane Strain," in *Solid Mechanics Part I: An Introduction to Solid Mechanics* (n.d.).
17. E. Hecht, "Chap 8: Polarization," in *Optics* (Pearson Education Limited, 2017).
18. P. D. Colbourne and D. T. Cassidy, "Imaging of stresses in GaAs diode lasers using polarization-resolved photoluminescence," IEEE Journal of Quantum Electronics **29**, 62–68 (1993).
19. R. A. Chipman, *Handbook of Optics, Volume II, Chap 22.15* (McGraw-Hill, New York, 1995).
20. M. Bass, *Handbook of Optics: Volume I-Geometrical and Physical Optics, Polarized Light, Components and Instruments* (McGraw-Hill Education, 2010).
21. G. G. Stoney, "The tension of metallic films deposited by electrolysis," Proceedings of the Royal Society of London. Series A, Containing Papers of a Mathematical and Physical Character **82**, 172–175 (1909).
22. S. J. Lascos and D. T. Cassidy, "Optical phase and intensity modulation from a rotating optical flat: effect on noise in degree of polarization measurements," Appl. Optics **48**, 1697–1704 (2009).